NJC

New Journal of Chemistry

A journal for new directions in chemistry

Accepted Manuscript

This article can be cited before page numbers have been issued, to do this please use: J. X. Li, Q. L. Guan, Y. Wang, Z. X. You, Y. Xing, F. Bai and L. Sun, *New J. Chem.*, 2020, DOI: 10.1039/C9NJ05175A.

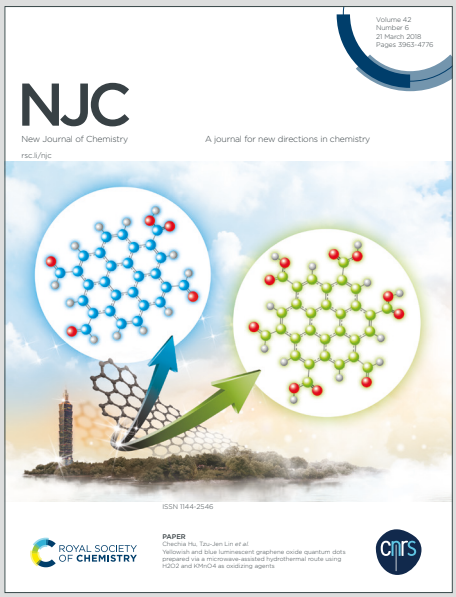

View Article Online
DOI: 10.1039/C9NJ05175A

Journal Name

ARTICLE

Received 00th January 20xx,

Accepted 00th January 20xx

DOI: 10.1039/x0xx00000x

www.rsc.org/

Lanthanide-Organic Crystalline Framework Material Encapsulated by 1,3,6,8-tetrakis (p-benzoic acid) pyrene: Selective Sensing on Fe^{3+}, $Cr_2O_7^{2-}$ and Colchicine and White-light Emission

Jin Xiao Li,[a] Qing Lin Guan,[a] Yu Wang,[a] Zi Xin You,[a] Yong Heng Xing,*[a] Feng Ying Bai,*[a] Li Xian Sun[b]

A facile strategy was used to construct a series of composite materials with color-tunable and white light emitting by encapsulating 1,3,6,8-tetrakis (p-benzoic acid) pyrene (H_4TBAPy) into framework material $[Eu(MCTCA)_{1.5}(H_2O)_2]\cdot1.75H_2O$ (Eu-MCTCA), which is synthesized based on $Eu(NO_3)_3\cdot6H_2O$ and 5-methyl-1-(4-carboxylphenyl)-1H-1,2,3-triazole-4-carboxylic acid (H_2MCTCA). A slight adjustment of the emitted color can be easily fulfilled by simply altering the concentration of H_4TBAPy or regulating the excitation wavelength. Notably, the white light emitting Eu-MCTCA@H_4TBAPy can be realized by encapsulating H_4TBAPy with a concentration of 0.75 mM, when the excitation wavelength is 350 nm. Furthermore, based on the favorable luminescence and stable structure of Eu-MCTCA@H_4TBAPy in water or organic solvents, the Eu-MCTCA@H_4TBAPy can be used as a potential luminescent probe for detecting of Fe^{3+}, $Cr_2O_7^{2-}$ and colchicine.

Introduction

Nitrogen-heterocyclic ligands have attracted extensive attention from researchers since the study of metal-organic coordination polymers, and the reason is that nitrogen-heterocyclic ligands show favorable coordination ability and varied coordination modes, which can form diverse coordination polymers with novel structures[1,2]. There are many kinds of heterocyclic ligands with rich configurations, the most common nitrogen-containing heterocyclic azoles are triazole, tetrazole and their derivatives[3-6]. Metal-organic frameworks (MOFs) are an emerging class of materials consisting of metal nodes/clusters and organic linkers[7]. Among them, MOFs are formed by connecting triazole or tetrazole to metal ions, especially rare earth ions, showing various structures and excellent physical and chemical properties[8]. Due to the organic ligands with nitrogen heterocycles have goodish sensitization to rare earth ions, unique electronic structures and luminescent properties[9], rare earth coordination frameworks constructed from nitrogen heterocyclic ligands usually have excellent properties[10]. At the same time, these rare earth coordination frameworks have many advantages with simple synthesis methods, designable structures and light-emitting diversity. All above make them widely used as functional materials in many fields, for instance, magnetic resonance imaging[11], optical devices[12], biomedical medicine[13-15], light control[16], magnetic[17, 18], gas absorption[19] and fluorescent sensors[20-22], which become a research hotspot in recent years.

Fe^{3+} and $Cr_2O_7^{2-}$ ions are two well-known important ions, in which Fe^{3+} ions play a crucial role in most organisms. For example, it is advantageous for storing and transporting oxygen, controlling muscle and brain functions, maintaining the balance of the immune system and the enzyme system etc.[23]. However, the lack or overload of Fe^{3+} ions can also cause various diseases, such as skin disorders, insomnia, anemia, liver damage, heart failure and Parkinson's disease[24]. While $Cr_2O_7^{2-}$ as an important oxidant in industry, it is extensive used in industry not only causes serious environmental degradation, but also endangers human health. It can cause skin ulcers, which in severe cases can lead to lung and gastrointestinal cancer[25-28]. Therefore, selective and accurate monitoring of Fe^{3+} or $Cr_2O_7^{2-}$ ions is of great significance. On the other hand, colchicine is a kind of natural alkaloid occurring in colchicum which can be used to treat gout and arthrophlogosis, but it is also very toxic to human beings[29,30]. As far as we know, there are many methods to detect colchicine. However, there are few reports to detection colchicine using MOFs as sensors.

Pyrene is a part of polycyclic aromatic hydrocarbons family and has the dual roles of electron donating and electron withdrawing[31,32]. Since Laurent discovered pyrene in the residue of coal tar destructive distillation in 1837, this polycyclic aromatic hydrocarbon has been the subject of extensive research[33]. Among many organic ligands, pyrene and its derivatives have many advantages such as high thermal stability, photochemical stability, pure blue fluorescence, plane geometry and natural high charge mobility[34-36]. They have attracted attention because they can be widely applied in Organic Light Emitting Display(OLEDs)[37-40], organic photovoltaic(OPVs)[41], organic electronic devices, nanomaterials[42,43] and chemical sensing[44]. At present, there are two main research directions for pyrene. One is to modify the active site of pyrene, such as Yamato *et al.* indicated that a -CHO group could selectively attach to 4- or 4,9- position of the pyrene under the different catalytic conditions of Lewis acid[45]. Charka *et al.* synthesized a novel pyrene emitting material for OLED devices by adding N-styrene-carbazole-branched chain units at positions 2 and 7[46]. The other line of research is to coordinate pyrene with metal ions. For instance, Li *et al.* synthesized three novel structures of MOFs by changing reaction conditions based on four dominant bodies (1,3,6,8-tetrakis (p-benzoic acid) pyrene) as the

College of Chemistry and Chemical Engineering, Liaoning Normal University, Huanghe Road 850#, Dalian 116029, P.R. China.
Guangxi Key Laboratory of Information Materials, Guilin University of Electronic Technology, Guilin City, 541004, P.R. China
** Corresponding author. E-mail address: xingyongheng2000@163.com (Y. H. Xing); baifengying2003@163.com (F. Y. Bai)*
†Electronic Supplementary Information (ESI) available. See DOI:10.1039/x0xx00000x

View Article Online
DOI: 10.1039/C9NJ05175A

linker. These MOFs are all constructed by rod-SBU and have novel topological network[47,48]. However, there are rare reports about pyrene doping to framework of the complexes. In this work, we have successfully synthesized a series of fluorescence-adjustable and structurally stable composite materials by encapsulating 1,3,6,8-tetrakis (p-benzoic acid) pyrene (H_4TBAPy) into $[Eu(MCTCA)_{1.5}(H_2O)_2]\cdot1.75H_2O$ (Eu-MCTCA). In the H_4TBAPy-encapsulated MOF system, the energy from the ligand to the central metal ion Eu^{3+} is reduced and the ability of Eu-MCTCA for detecting and recognize colchicine, Fe^{3+} and $Cr_2O_7^{2-}$ is improved.

Experimental

Materials and Methods

Eu_6O_{11} was purchased from Shanghai Aladdin Biochemical Technology co. LTD. Ethanol and Nitric acid were purchased from Tianjin Comio Chemical Reagent Co. LTD. All raw materials were used directly without further purification. Structural characterization of the composites using infrared spectrometer (JASCO V-570 Fourier transform), UV-visible spectrophotometer (Lambda 35) and X-ray powder diffractometer (Bruker Advance-D8). Fluorescence spectrometer (HORIBA Fluoromax-4-TCSPC) was used to study the properties of the composites. Composite materials before and after encapsulating H_4TBAPy were determined by elemental analysis using organic element analyser (Vario EL CVBE). The scanning electron microscope (SEM) image and Atomic force microscopy (AFM) images were acquired using SU8010 scanning electron microscope (HITACHI, Tokyo, Japan) and Cypher ES platform (Asylum Research, Oxford Instruments, USA), respectively.

Synthesis of H_4TBAPy and ligand H_2MCTCA

1,3,6,8-tetrakis (p-benzoic acid) pyrene (H_4TBAPy)[49,50] and 5-methyl-1-(4-carboxylphenyl)-1H-1,2,3-triazole-4-carboxylic acid (H_2MCTCA)[51,52] were synthesized according to previous literature. The synthetic process of the H_4TBAPy and ligand H_2MCTCA is shown in **Supplementary Information.** The ^{1}H-NMR, ^{13}C-NMR and HRMS spectra of H_2MCTCA are shown in Figure S1-S3 and the ^{1}H-NMR of H_4TBAPy spectrum is shown in Figure S4.

Synthesis of Eu-MCTCA

$[Eu(MCTCA)_{1.5}(H_2O)_2]\cdot1.75H_2O$ (Eu-MCTCA) was synthesized by the hydrothermal reaction according to a previously reported literature[53]. $Eu(NO_3)_3\cdot6H_2O$ (0.1 mM, 0.043 g) and H_2MCTCA (0.05 mM, 0.01 g) were dissolved in 2 mL water and 5 mL ethanol solution, respectively. After stirring for 2 hours, the solution was sealed in 25 mL stainless steel autoclave. It was heated at 100 °C for 4 days and cooled at room temperature to produce colorless crystals.

Preparation of Eu-MCTCA@H_4TBAPy Composites

The composite material Eu-MCTCA@H_4TBAPy was based on the synthesis of coordination polymer Eu-MCTCA. The specific synthesis process was shown in Figure 1. The as-prepared Eu-MCTCA (20 mg) was soaked into DMF solutions containing four kinds of the different concentrations of H_4TBAPy at the room temperature. The concentration of H_4TBAPy was 0.15 mM (Eu-MCTCA@H_4TBAPy-0.15), 0.30 mM (Eu-MCTCA@H_4TBAPy-0.30), 0.60 mM (Eu-MCTCA@H_4TBAPy-0.60) and 0.75 mM (Eu-MCTCA@H_4TBAPy-0.75), respectively. Soaked in the dark for 24 hours, the composites were washed thoroughly with DMF (5 mL × 5), and then dried at room temperature for 24 h.

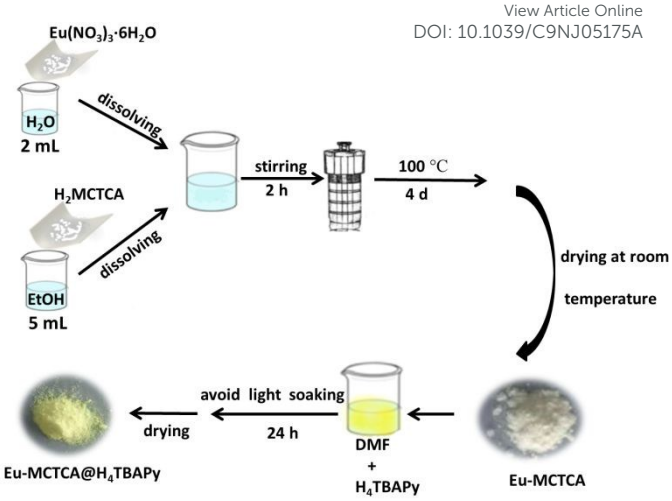

Figure 1 Schematic diagram for the preparation of Eu-MCTCA and Eu-MCTCA@H_4TBAPy.

Luminescence Regulation of Eu-MCTCA@H_4TBAPy Composites

Four different concentrations of H_4TBAPy were encapsulated in Eu-MCTCA to get the composites and then solid composites were excited with different excitation wavelengths to obtain fluorescence emission spectra.

Fluorescence Quenching and Titration Experiments

To study the sensing ability of Eu-MCTCA@H_4TBAPy towards eleven different metal ions (Ag^+, Ba^{2+}, Ca^{2+}, Co^{2+}, Cu^{2+}, Fe^{3+}, K^+, Mg^{2+}, Na^+, Ni^{2+} and Pb^{2+}) and eleven different anions (Br^-, CH_3COO^-, CO_3^{2-}, $Cr_2O_7^{2-}$, HCO_3^-, I^-, MnO_4^-, NO_2^-, NO_3^-, $S_2O_3^{2-}$ and SO_4^{2-}). 20 mg fully ground powder of Eu-MCTCA@H_4TBAPy-0.75 composites were soaked in 100 mL absolute ethanol and sonicated for about 40 min to prepare a well-dispersed suspension of composite. Afterwards, 160 μL of 10^{-2} M aqueous solutions of the anions and metal ions were added respectively to 3 mL the as-prepared suspension in cuvettes. In titration experiments, Fe^{3+} or $Cr_2O_7^{2-}$ aqueous solution (10^{-2} M) was added to 3 mL of Eu-MCTCA@H_4TBAPy-0.75 suspension in a same incremental manner. All fluorescence spectra were measured at room temperature. The Stern-Volmer formula for calculating quenching rate is $(I_0/I) = 1 + K_{sv}[Q]$, where I_0 is the fluorescence emission intensity of Eu-MCTCA@H_4TBAPy-0.75 without adding testing sample, I is the fluorescence emission intensity of Eu-MCTCA@H_4TBAPy-0.75 suspension after adding testing sample, K_{sv} is the quenching rate constant (M^{-1}), [Q] represents the molar concentration of testing sample.

The detection of colchicine by the Eu-MCTCA@H_4TBAPy-0.75 composite is similar to the method of detecting metal ions and anions. 20 mg powder sample of Eu-MCTCA@H_4TBAPy-0.75 was soaked in 50 mL absolute ethanol and sonicated for 40 minutes, then 3 mL the Eu-MCTCA@H_4TBAPy-0.75 suspension was added to the cuvette. Fluorescence sensing research was carried out by adding colchicine solution with a concentration of 1 mM to the suspension that the fluorescence emission intensity was measured and compared.

View Article Online
DOI: 10.1039/C9NJ05127A

Results and discussion

Eu-MCTCA was synthesized according to the methods reported in previous literature. As shown in Figure S5, the diffraction peaks of the synthesized Eu-MCTCA agree well with the simulated Eu-MCTCA diffraction peaks, indicating that the Eu-MCTCA crystal was successfully prepared. At the same time, in Figure S5, we also found that the peak position of Eu-MCTCA@H_4TBAPy was completely consistent with that of Eu-MCTCA, indicating that the main structure of Eu-MCTCA was not changed after the H_4TBAPy is encapsulated. According to the crystal structure of Eu-MCTCA, the skeleton contains two channels of different sizes along the c-axis, which are 13.85 Å × 13.05 Å and 23.6 Å × 12.1 Å. The size of H_4TBAPy is 12.72 Å × 12.46 Å. Theoretically, H_4TBAPy can enter the Eu-MCTCA channel. However, considering that the Eu-MCTCA channels have a large degree of distortion, we thought that the few amount of H_4TBAPy enter the channels. The vast majority of H_4TBAPy molecules are closely connected with the Eu-MCTCA frameworks by surface interaction of π···π or hydrogen bond. To prove this conjecture, we carried out further experiments.

After soaking in DMF solution of H_4TBAPy of different concentrations, the color change of particles is apparent (Figure S6), which proves that the H_4TBAPy molecules were coupled with the Eu-MCTCA host[54]. From the SEM image of Eu-MCTCA (Figure 2a), it can be seen that its morphology is all lumpy and uniformly distributed. After encapsulating H_4TBAPy (Figure 2b), its morphology turns into a microstructure similar to fiber strip, indicating the presence of H_4TBAPy on the surface of Eu-MCTCA. In the IR spectra(Figure S7), we found that there was no influence on the peak shape and position of Eu-MCTCA before and after encapsulating the H_4TBAPy. The UV-vis spectra of Eu-MCTCA and Eu-MCTCA@H_4TBAPy were shown in Figure S8, it can be concluded that the absorption peaks in the 200-330 nm originates from the π→π* transition of Eu-MCTCA. The absorption peaks in the 400 nm roots in the H_4TBAPy of the π→π* and n→π* transition. The absorption band in 400 nm of the Eu-MCTCA@H_4TBAPy is narrower than that of the H_4TBAPy, indicating that there was an interaction between Eu-MCTCA and H_4TBAPy. The Figure S9 is the solid-state luminescent spectra for H_2MCTCA (a), Eu-MCTCA (b) and Eu-MCTCA@H_4TBAPy (c) at room temperature. In Figure S9b, the excitation spectrum of Eu-MCTCA showed a broad band at about 370-400 nm, when the excitation wavelength was 390 nm, the emission spectrum of Eu-MCTCA showed clear luminescence of f-f transition, which was due to the energy transfer from H_2MCTCA ligand to Eu^{3+} ions[55]. There are four characteristic emission peaks of Eu^{3+} in the emission spectrum of Eu-MCTCA. Among them, the strongest emission occurs at 614 nm ($^5D_0$-$^7F_2$), other lower characteristic peaks were simultaneously concentrated in 586/590 ($^5D_0$-$^7F_1$), 650 ($^5D_0$-$^7F_3$) and 686/692 nm ($^5D_0$-$^7F_4$). Double peaks are generated due to the high symmetry environment of Eu^{3+}[56]. In addition, we also observed the excimer emission peak of chromophore pyrene in H_4TBAPy at around 460 nm from the emission spectrum of Eu-MCTCA@H_4TBAPy, indicating that H_4TBAPy is present in the Eu-MCTCA@H_4TBAPy[57]. The results of elemental analysis also show that the presence of H_4TBAPy increases the content of H and C, while decreases the content of N. (Eu-MCTCA: C, 33.49%; H, 2.47%; N, 10.96%. Eu-MCTCA@H_4TBAPy: C, 34.39%; H, 2.51%; N, 10.42%) According to the above results, the H_4TBAPy molecules were successfully encapsulated in Eu-MCTCA.

In order to verify the binding stability of the H_4TBAPy with the Eu-MCTCA host, the H_4TBAPy and Eu-MCTCA@H_4TBAPy were dispersed in DMF and treated by sonication for 2 min, Figure 3 shown that the supernatant of Eu-MCTCA@H_4TBAPy after sonication did not emit light under the 365 nm UV irradiation, suggesting that few H_4TBAPy molecules were detached from the Eu-MCTCA@H_4TBAPy host. In addition, the supernatant of sonication treated H_4TBAPy still has strong fluorescence emission intensity, while the supernatant of Eu-MCTCA@H_4TBAPy has almost no fluorescence emission intensity (Figure S10). It is seen that the H_4TBAPy molecules are closely connected with the Eu-MCTCA frameworks.

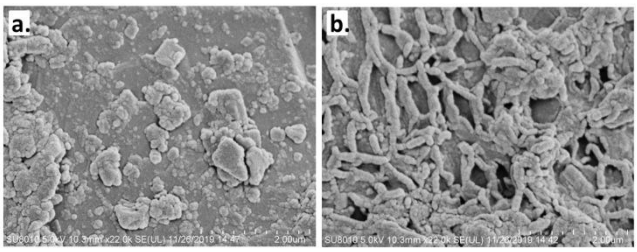

Figure 2 **a.** SEM image of Eu-MCTCA (2 μm); **b.** SEM image of Eu-MCTCA@H_4TBAPy-0.75 (2 μm).

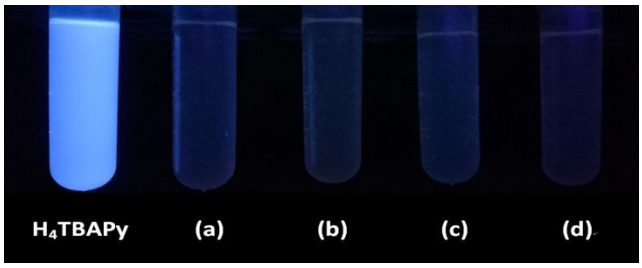

Figure 3 Photographs of H_4TBAPy, Eu-MCTCA@H_4TBAPy-0.15(a), Eu-MCTCA@H_4TBAPy-0.30(b), Eu-MCTCA@H_4TBAPy-0.60(c), and Eu-MCTCA@H_4TBAPy-0.75(d) supernatant after sonicating for 2 min under 365 nm UV irradiation.

In the experiment of luminescence adjustment (Figure 4), it was found that the intensity of the characteristic emission peak of the Eu^{3+} gradually increased with the increasing concentration of H_4TBAPy. This may be due to the formation of a π→π* interaction between the H_4TBAPy and the ligand in the coordination frameworks. The energy of ligand transfers to Eu^{3+} is increased, thus lead to the fluorescence intensity is enhanced. The characteristic emission peaks of Eu^{3+} and the fluorescence intensity of H_4TBAPy are different for the same composite under the different excitation wavelengths, which leads to different CIE color coordinates. The specific CIE color coordinates are listed in Table S1. The specific CIE chromaticity diagrams show in Figure S11. It can be seen that most of composites with different contents of H_4TBAPy at different excitation wavelengths can obtain color coordinates close to white light. The most notable among that when the Eu-MCTCA is encapsulated with 0.75 mM of H_4TBAPy and excited by a wavelength of 350 nm, the best near-white emission with a color coordinate of (0.3482, 0.3301) can be obtained.

So as to test the ability of the Eu-MCTCA@H_4TBAPy-0.75 to detect trace metal ions, the fluorescence sensing and titration experiments were carried out. The experimental results are as follows (Figure S12). It is found that the fluorescence intensity of Eu-MCTCA@H_4TBAPy-0.75 depends largely on the species of metal ions. Fe^{3+} shows obvious fluorescence quenching effect, while the

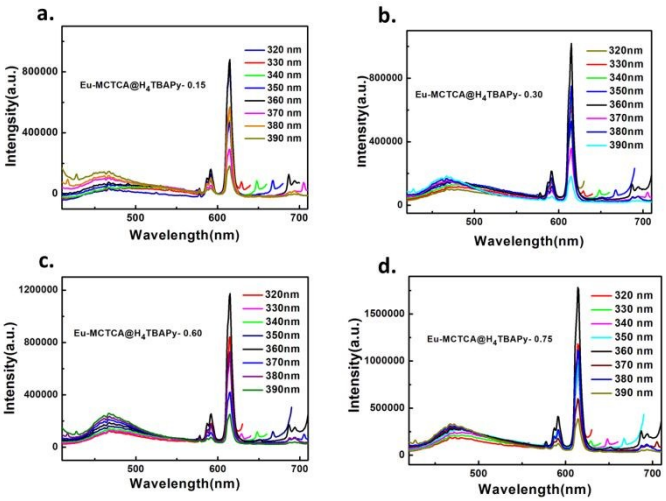

Figure 4 Fluorescence spectra of composites with different contents of H_4TBAPy at different excitation wavelengths. (**a.** Eu-MCTCA@H_4TBAPy-0.15, **b.** Eu-MCTCA@H_4TBAPy-0.30, **c.** Eu-MCTCA@H_4TBAPy-0.60 and **d.** Eu-MCTCA@H_4TBAPy-0.75)

effect of other metal ions on fluorescence can be neglected. In the next moment, further sensitivity experiment was conducted out by adding gradually Fe^{3+} aqueous solution to the ethanol of Eu-MCTCA@H_4TBAPy-0.75. As shown in Figure 5a, the emission intensity of Eu-MCTCA@H_4TBAPy-0.75 at 615 nm decreased with increasing of concentration of Fe^{3+}. When the concentration of Fe^{3+} is relatively high, there is a very good linear relationship between the I_0/I and concentration of Fe^{3+}. The K_{sv} value was calculated to be 2.01×10^4 M^{-1} (Figure S13), furthermore, the detection limit of Eu-MCTCA@H_4TBAPy-0.75 toward Fe^{3+} to be 3.06 μM. Table S2 lists the K_{sv} values of some lanthanide metal coordination polymer materials for the detection of Fe^{3+} ions by fluorescence sensing. Compared with the previously reported K_{sv} value of lanthanide based light-emitting sensors, the K_{sv} value of the Eu-MCTCA@H_4TBAPy is higher than that of most sensors. The higher quenching efficiency K_{sv} value indicates that the Eu-MCTCA@H_4TBAPy pairs have higher sensitivity to detect Fe^{3+} ions, which makes Eu-MCTCA@H_4TBAPy one of the better fluorescence detectors for detecting Fe^{3+}. The high selectivity of the Eu-MCTCA@H_4TBAPy for the detection of Fe^{3+} was further proved by interference experiments. Add 100 μL of 10^{-2} M different metal solutions to the ethanol suspension of Eu-MCTCA@H_4TBAPy-0.75, and then add 100 μL of 10^{-2} M Fe^{3+} aqueous solution. Interestingly, the fluorescence intensity was significantly quenched after the addition of Fe^{3+} ions (Figure S14). The change of luminescence intensity after adding different metal ions at 614 nm is shown in Figure 5b. The experimental results show that the presence of other competitive metal ions does not affect the detection of Fe^{3+} by Eu-MCTCA@H_4TBAPy.

For the detection of anions, the same method as the detection of metal ions was employed. As shown in Figure S15, it can be observed that different anions have different effects on the fluorescence intensity of the Eu-MCTCA@H_4TBAPy-0.75. The addition of most anions has little effect on the fluorescence intensity of Eu-MCTCA@H_4TBAPy-0.75. However, after added $Cr_2O_7^{2-}$, the Eu-MCTCA@H_4TBAPy-0.75 has significant fluorescence quenching. Sensitivity experiment was further carried out by adding $Cr_2O_7^{2-}$ gradually to disperse in ethanol of Eu-MCTCA@H_4TBAPy-0.75. As shown in Figure 6a, the emission intensity of Eu-MCTCA@H_4TBAPy-0.75 at 615 nm decreases with increasing concentration of $Cr_2O_7^{2-}$. The K_{sv} value of Eu-MCTCA@H_4TBAPy-0.75 for $Cr_2O_7^{2-}$ was calculated to be 1.69×10^5 M^{-1} (Figure S16), and the detection limit of Eu-MCTCA@H_4TBAPy-0.75 toward $Cr_2O_7^{2-}$ was 0.58 μM. Table S3 lists the K_{sv} values of some lanthanide metal coordination polymer materials for the detection of $Cr_2O_7^{2-}$ by fluorescence sensing. That the quenching rate constant K_{sv} of Eu-MCTCA@H_4TBAPy-0.75 $Cr_2O_7^{2-}$ probe can reach 10^5 M^{-1}. According to the literature, most reported the K_{SV} of MOFs detection $Cr_2O_7^{2-}$ is generally 10^2 to 10^4 M^{-1}, and the present results indicate that the Eu-MCTCA@H_4TBAPy-0.75 could behave as a highly sensitive luminescence sensor for detection of $Cr_2O_7^{2-}$ in aqueous solution. Using the same method as Fe^{3+}, the interference experiment is carried out on $Cr_2O_7^{2-}$. The fluorescence intensity was significantly quenched after the addition of $Cr_2O_7^{2-}$ ions (Figure S17). The change of luminescence intensity after adding different anions at 614 nm is shown in Figure 6b. The presence of other competitive anions does not affect the detection of $Cr_2O_7^{2-}$ by Eu-MCTCA@H_4TBAPy-0.75, indicating that Eu-MCTCA@H_4TBAPy-0.75 is highly selective in the detection of $Cr_2O_7^{2-}$.

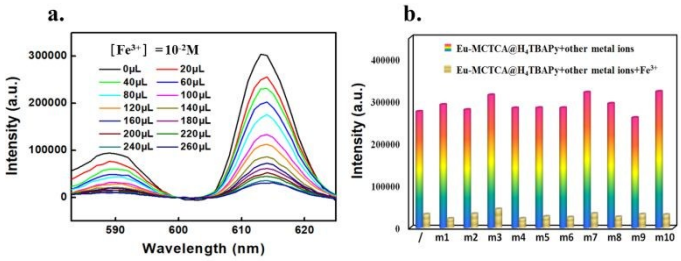

Figure 5 **a.** Change of fluorescent emission spectra of the Eu-MCTCA@H_4TBAPy-0.75 dispersed in ethanol upon with gradually adding Fe^{3+} aqueous solution (λex= 360 nm). **b.** The change of luminescence intensities at 614 nm upon addition of different metal ions. (**m1:** Ba^{2+}, **m2:** Ca^{2+}, **m3:** Ag^{+}, **m4:** Co^{2+}, **m5:** Cu^{2+}, **m6:** K^{+}, **m7:** Mg^{2+}, **m8:** Na^{+}, **m9:** Ni^{2+}, **m10:** Pb^{2+})

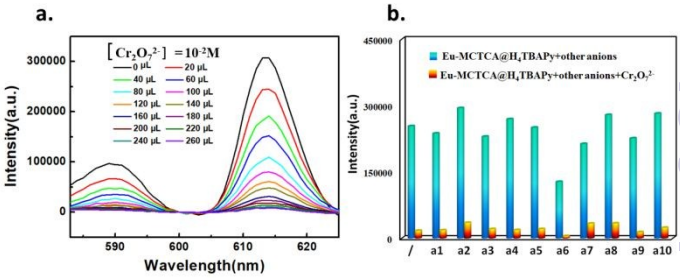

Figure 6 **a.** Change of fluorescent emission spectra of the Eu-MCTCA@H_4TBAPy-0.75 dispersed in ethanol upon with gradually adding $Cr_2O_7^{2-}$ aqueous solution (λex= 360 nm). **b.** The change of luminescence intensities at 614 nm upon addition of different anions. (**a1:** Br^{-}, **a2:** CH_3COO^{-}, **a3:** CO_3^{2-}, **a4:** HCO_3^{-}, **a5:** I^{-}, **a6:** MnO_4^{-}, **a7:** NO_2^{-}, **a8:** NO_3^{-}, **a9:** $S_2O_3^{2-}$, **a10:** SO_4^{2-})

There are more and more detection methods for colchicine with the development of analytical techniques[58]. Because Eu-MCTCA has good fluorescence properties, we studied the detection ability of Eu-MCTCA, H_4TBAPy and Eu-MCTCA@H_4TBAPy-0.75 to trace colchicine. First, we studied the ability of Eu-MCTCA to detect colchicine, as shown in Figure 7, we observed that fluorescence intensity of the system is quench significantly with the increase of the concentration of colchicine. In other words, their fluorescence intensity is affected greatly by the concentration of colchicine solution. The K_{sv} value of Eu-MCTCA to colchicine was calculated

View Article Online
DOI: 10.1039/C9NJ05175A

to be 1.32×10^4 M^{-1}. At the same time, we studied the fluorescence sensing detection of H_4TBAPy for infinitesimal colchicine. As shown in Figure 8, the fluorescence intensity of H_4TBAPy decreased with the increase of colchicine's content in the system when the concentration of colchicine is 1 mM. The K_{sv} value of H_4TBAPy for colchicine was 2.01×10^4 M^{-1}, the detection effect is obviously better than Eu-MCTCA. In addition, we also used the same method to study the ability of Eu-MCTCA@H_4TBAPy-0.75 to detect colchicine. As shown in Figure 9, fluorescence emission spectra of the colchicine were obtained under the excitation of the wavelength of 350 nm. It can be seen that the Eu-MCTCA@H_4TBAPy-0.75 has a higher K_{sv} value of 3.49×10^4 M^{-1} to detect colchicine, so the detection sensitivity is the highest, and the detection limit of Eu-MCTCA@H_4TBAPy-0.75 toward colchicine was 1.68 μM. As shown in Figure 10, K_{sv} values of colchicine detected by Eu-MCTCA, H_4TBAPy and Eu-MCTCA@H_4TBAPy-0.75 increased gradually. From what has been discussed above, it can be seen that the ability of Eu-MCTCA to detect and recognize colchicine was improved after encapsulating H_4TBAPy.

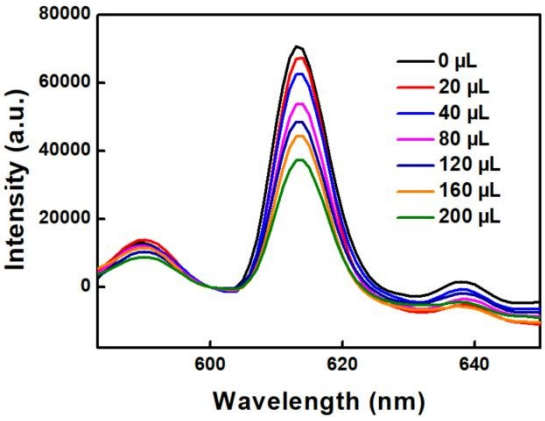

Figure 7 Fluorescence emission spectra of Eu-MCTCA for detecting colchicine (λex=390 nm).

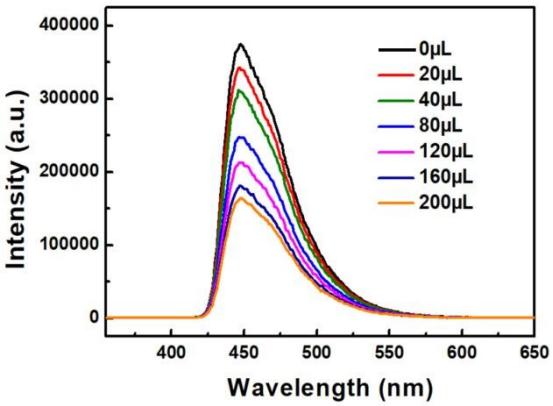

Figure 8 Fluorescence emission spectra of H_4TBAPy for detecting colchicine (λex= 335 nm).

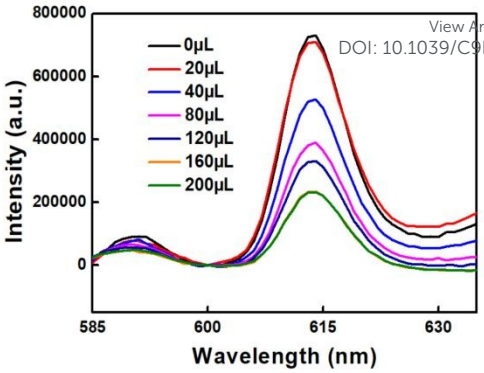

Figure 9 Fluorescence emission spectra of Eu-MCTCA@H_4TBAPy-0.75 for detecting colchicine (λex=350 nm).

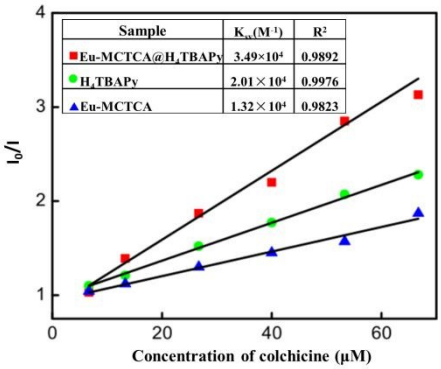

Figure 10 Plot of fraction of luminescence emission intensity vs concentration of analytes for Eu-MCTCA, H_4TBAPy and Eu-MCTCA@H_4TBAPy-0.75.

The mechanism of luminescent response

In order to further clarify the detection mechanism of the sensor, we measured the PXRD spectra of Eu-MCTCA@H_4TBAPy soaked in Fe^{3+}, $Cr_2O_7^{2-}$ and colchicine aqueous solutions for 24 h. According to the PXRD spectra (Figure S18), it is found that Fe^{3+}, $Cr_2O_7^{2-}$ and colchicine did not destroy the skeleton structure of Eu-MCTCA@H_4TBAPy, so the possibility of fluorescence quenching caused by skeleton collapse was ruled out. SEM images were used to characterize the topography of Eu-MCTCA@H_4TBAPy before and after detection, before adding the analyte (Figure 11a), its morphology was similar to that of fiber strips and its distribution was relatively uniform. However, after the addition of the analyte (Figure 11b-d), the part of the complex molecular agglomerate and changed from strips to blocks, with the addition of $Cr_2O_7^{2-}$ and colchicine being the most obvious. In addition, the atomic force microscope (AFM) was also used to characterize the morphological changes of Eu-MCTCA@H_4TBAPy before and after the detection. Figure 12 shows the 2D (20 μm×20 μm) and 3D images of the AFM. It can also be seen that the surface molecules of Eu-MCTCA@H_4TBAPy after detection are relatively more aggregated than those before detection. This indicates that Fe^{3+}, $Cr_2O_7^{2-}$ or colchicine may have some effect on the coordination spheres of Eu^{3+} in Eu-MCTCA.

As we all known that the fluorescence intensity of rare earth ions is mainly determined by the energy transfer from the ligands to Ln^{3+}[59,60]. If there is effective energy transfer within the molecule, Ln^{3+} can be more effectively stimulated, resulting in enhanced lanthanide luminescence, and vice versa, resulting in reduced luminescence. It is predicted that the addition of detectors will affect the efficiency of energy conversion between H_4TBAPy, H_2MCTCA and Ln^{3+}, resulting in enhanced fluorescence

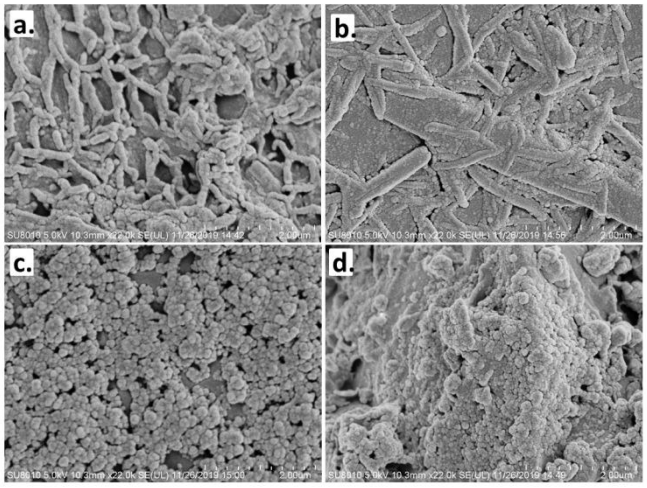

Figure 11 SEM images of Eu-MCTCA@H_4TBAPy-0.75(a); Eu-MCTCA@H_4TBAPy-0.75 for detecting Fe^{3+}(b); Eu-MCTCA@H_4TBAPy-0.75 for detecting $Cr_2O_7^{2-}$(c); Eu-MCTCA@H_4TBAPy-0.75 for detecting colchicine(d); (2 μm).

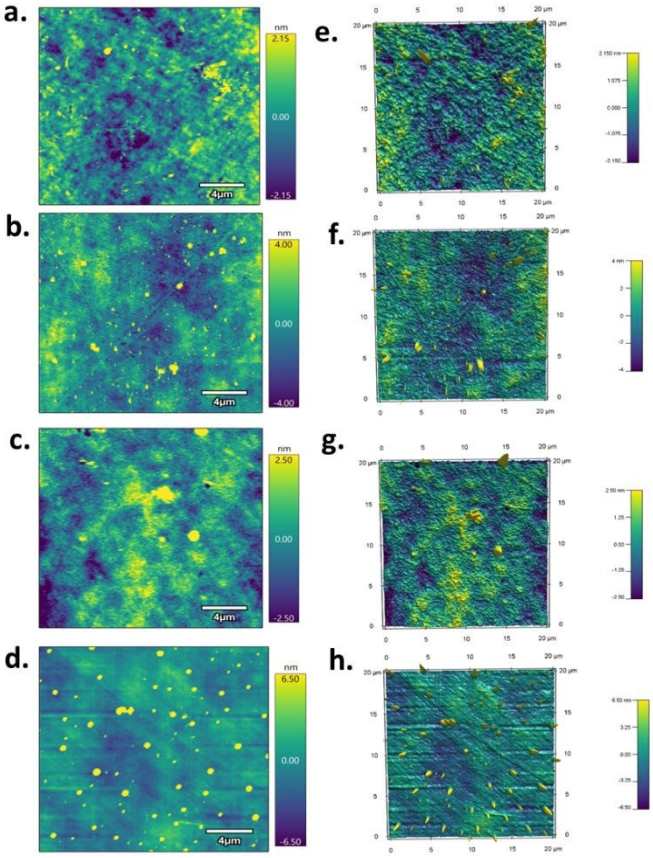

Figure 12 Atomic force microscope images of the surface for Eu-MCTCA@H_4TBAPy-0.75(a); Eu-MCTCA@H_4TBAPy-0.75 for detecting Fe^{3+}(b); Eu-MCTCA@H_4TBAPy-0.75 for detecting $Cr_2O_7^{2-}$(c); Eu-MCTCA@H_4TBAPy-0.75 for detecting colchicine(d); (scan size 20 μm×20 μm). Atomic force microscope images of the 3D for Eu-MCTCA@H_4TBAPy-0.75(e); Eu-MCTCA@H_4TBAPy-0.75 for detecting Fe^{3+}(f); Eu-MCTCA@H_4TBAPy-0.75 for detecting $Cr_2O_7^{2-}$(g); Eu-MCTCA@H_4TBAPy-0.75 for detecting colchicine(h).

and quenching[61-64]. In order to explore the detection mechanism of analyte and Eu-MCTCA@H_4TBAPy, firstly, comparison of the UV-vis spectra of analytes and the emission spectra of Eu-MCTCA@H_4TBAPy-0.75 was analyzed (Figure S19). Among them, we used different excitation wavelengths to excite Eu-MCTCA@H_4TBAPy-0.75 in order to obtain a complete emission spectrum. When the excitation wavelength is 300 nm, we get the fluorescence emission peak of the H_2MCTCA moiety at 340 nm. Similarly, at the excitation wavelength of 390 nm, we observed the excimer emission peak of chromophore pyrene in H_4TBAPy moiety at around 460 nm and the characteristic emission of Eu^{3+} at 590 and 614 nm. Compared with the emission spectrum of Eu-MCTCA@H_4TBAPy-0.75, the UV-vis spectra of the analyte partially overlap with the emission spectrum of Eu-MCTCA@H_4TBAPy. The main part of the overlap occurs at the position of the fluorescence emission peak of the H_2MCTCA moiety. This shows that there is energy transfer between the H_2MCTCA moiety and the analyte, which leads to a decrease in energy transfer from H_2MCTCA moiety to Eu^{3+} ions and quenches the fluorescence of Eu-MCTCA@H_4TBAPy-0.75. Secondly, we also measured the fluorescence lifetime of corresponding to each stage. The specific data are listed in Table S4. After packaging H_4TBAPy, the solid fluorescence lifetime of Eu-MCTCA@H_4TBAPy-0.75 is still a single exponential decay process (Figure S20). After adding the analyte (Figure S21-S24), the fluorescence lifetime of the composite is reduced. The results show that these processes are dynamic quenching processes, which reduces the energy transfer of the ligand to Eu^{3+}.

In addition, the competition of energy is also a possible cause of the fluorescence quenching phenomenon. If the excitation spectrum of the fluorophore (donor) overlaps with the absorption spectrum of the analyte (acceptor) to some extent, there may be a competitive energy absorption process between the ligand and the analyte solution[65]. Therefore, we studied the excitation spectrum of Eu-MCTCA@H_4TBAPy and the ultraviolet spectrum of the aqueous solution of the analyte, and plotted the corresponding spectra (Figure S25). Similarly, in order to obtain a complete excitation spectrum, different monitoring peaks were used to measure the excitation spectrum. Under the monitoring of 460 nm, the electronic transitions attributable to H_2MCTCA and H_4TBAPy with a width peak of 300-400 nm were obtained. Under 614 nm monitoring, sharp peaks at 465 and 540 nm were obtained due to the strong transition of the Eu^{3+} energy level. The Figure 14 show that the UV-vis spectra of the analyte partially overlap with the excitation spectrum of Eu-MCTCA@H_4TBAPy. This indicates that there is energy competition between the analyte, H_2MCTCA moiety and H_4TBAPy moiety, so the reason for fluorescence quenching is that the energy was absorbed by H_2MCTCA moiety and H_4TBAPy moiety, and the energy transferred to Eu^{3+} decreases. In addition, we also measured the UV-vis spectra of H_4TBAPy in DMF solution and Eu-MCTCA@H_4TBAPy in aqueous solution. In Figure S26, the absorption bands for H_4TBAPy observed in the UV region (between 248 and 298 nm) are caused by the $S_0 \rightarrow S_3$ transition in the pyrene units. The broad absorption bands located at 389 nm can be ascribed to n–π* transitions of pyrene[66]. In Figure S27, it is found that the UV-vis spectra also overlap, further confirming the competition for energy between the analyte and Eu-MCTCA@H_4TBAPy. In general, the main cause of fluorescence quenching is not only the energy transfer but also the energy competition between the analyte and H_2MCTCA moiety, which ultimately reduces the energy transferred to Eu^{3+} by the ligand.

Conclusions

In summary, the composites Eu-MCTCA@H_4TBAPy with high fluorescence emission intensity and trams form emission colors were successfully synthesized by the organic combination of H_4TBAPy and Eu-MCTCA. It can be proved that H_4TBAPy was successfully encapsulated in Eu-MCTCA by a series of characterization methods such as XRD, UV-vis and IR spectra. By changing the concentration of H_4TBAPy and excitation wavelength, the emission color gradually approaches white until emits white light. The composites could be effectively used in the detection of Fe^{3+} and $Cr_2O_7^{2-}$ with unique selectivity and sensitivity. The quenching constant K_{sv} were calculated to be 2.01×10^4 M^{-1} and 1.07×10^5 M^{-1}, respectively, and the detection limits are calculated as 3.06 μM and 0.58 μM respectively. It's worth noting that fluorescence intensity of Eu-MCTCA@H_4TBAPy can be quenched rapidly in a few seconds by the aqueous solution of colchicine. In addition, the result was confirmed by fluorescence quenching and titration, the Eu-MCTCA@H_4TBAPy-0.75 possesses excellent sensitivity and selectivity for colchicine and the value of K_{sv} is 3.49×10^4 M^{-1}, and the detection limit of Eu-MCTCA@H_4TBAPy-0.75 toward colchicine was 1.68 μM. These results suggest that sensitivity of Eu-MCTCA to Fe^{3+}, $Cr_2O_7^{2-}$ and colchicine could be improved by encapsulating H_4TBAPy. Besides, the Eu-MCTCA@H_4TBAPy would be a potential luminescent material for white LED.

Acknowledgements

This work was supported by the grants of the National Natural Science Foundation of China (No. 21571091), and Guangxi Key Laboratory of Information Materials, Guilin University of Electronic Technology, P.R. China (Project No.191001-K).

References

1. H. H. Zhao, N. Lopez, A. Prosvirin, H. T. Chifotides and K. R. Dunbar, Dalton Trans., 2007, **8**, 878-888.
2. M. Fumanal, F. Jiménez-Grávalos, J. Ribas-Arino and S. Vela, J. Am. Chem. Soc., 2017, **56**, 4474-4483.
3. X. W. Wu, F. Pan, S. Yin, J. Y. Ge, G. X. Jin, P. Wang and J. P. Ma, CrystEngComm., 2018, **20,** 3955-3959.
4. W. Liu, Y. L. Wang, L. Song, M. A. Silver, J. Xie, L. Zhang and S. Wang, Talanta., 2019, **196**, 515-522.
5. M. McCan, R. M. T. Casey, M. DeverEux, M. Curran, C. Cardin and A. Todd, Polyhedron., 1996, **15**, 2117-2120.
6. H. Winning, F. H. Larsen, R. Bro and S. B. Engelsen, Journal of Magnetic Resonance., 2008, **190**, 26-32.
7. Y. X. Wang, X. Liu, X. Y. Li, F. W. Zhai, S. q. Yan, N. Liu, Z. F. Chai, Y. D. Xu, X. P. Ouyang, S. A. Wang, J. Am. Chem. Soc., 2019, **141**, 8030-8034.
8. Y. Hasegawa, T. Nakanishi, RSC Advances., 2015, **5**, 338-353.
9. D. F. Sava, L. E. S. Rohwer, M. A. Rodriguez, M. A. Rodriguez and T. M. Nenoff, J. Am. Chem. Soc., 2012, **134**, 3983-3986.
10. Z. Q. Xia, Q. Wei, Q. Yang, C. Qiao, S. Chen, G. Xie and S. Gao, CrystEngComm., 2013, **15**, 86-99.
11. R. Nishiyabu, N. Hashimoto, T. Cho, K. Watanabe, T. Yasunaga, A. Endo and N. Kimizuka, J. Am. Chem. Soc., 2009, **131**, 2151-2158.
12. Y. X. Wang, X. M. Yin, W. Liu, J. Xie, J. F. Chen, Mark A. Silver, D. P. Sheng, L. H. Chen, J. Diwu, N. Liu, Z. F. Chai, E. Thomas, Albrecht-Schmitt, S. A. Wang, Angew. Chem. Int.Edit., 2018, **57**, 7883-7887.
13. M. D. Rowe, D. H. Thamm, S. L. Kraft and S. G. Boyes, Biomacromolecules., 2009, **10**, 983-993.
14. D. Xu, X. Y. Hao, Y. J. Shi, Z. K. Wang, Y. Li, W. T. Su and G. W. Yang, J. Coord. Chem., 2018, **71**, 1084-1092.
15. X. Huixia, W. Fang, W. Kexiang, S. Peng, L. Jie, Y. Tingting and X. Bingshe, Dyes and Pigments., 2017, **146**, 316-322.
16. C. Y. Lee, O. K. Farha, B. J. Hong, A. A. Sarjeant, S. T. Nguyen and J. T. Hupp, J. Am. Chem. Soc., 2011, **133**, 15858-15861.
17. L. Liang, G. Peng, L. Ma, L. Sun, H. Deng, H. Li and W. Li, Cryst. Growth Des., 2012, **12**, 1151-1158.
18. T. D. Pasatoiu, M. Etienne, A. M. Madalan, M. Andruh and R. Sessoli, Dalton Trans., 2010, **39**, 4802-4808.
19. W. Liu, X. Dai, Z. L. Bai, Y. L. Wang, Z. X. Yang, L. J. Zhang, L. Xu, L. H. Chen, Y. X. Li, D. X. Gui, J. Diwu, J. Q. Wang, R. H. Zhou, Z. F. Chai, S. A. Wang, Environ Sci. Technol., 2017, **51**, 3911-3921.
20. H. Zhang, J. Ma, D. Chen, H. Zhang, S. Zhang, W. Shi and P. Cheng, J. Mater. Chem. A., 2014, **2**, 20450-20453.
21. J. Xie, Y.X. Wang, W. Liu, X. M. Yin, L. H. Chen, Y. M. Zou, J. Diwu, Z.F. Chai, E. Thomas, Albrecht-Schmitt, G. K. Liu, S.A. Wang, Angew. Chem. Int. Ed., 2017, **56**, 7500-7504.
22. W. Liu, X. Dai, Y. L. Wang, L. P. Song, L.. J. Zhang, D. Zhang, J. Xie, L. Chen, J. Diwu, J. Q. Wang, Z. F. Chai, S. A. Wang, Environ Sci. Technol., 2019, **53**, 332-341.
23. L. M. Hyman, K. J. Franz, Coord. Chem. Rev., 2012, **256**, 2333-2356.
24. T. N. Duc, R. E. Zein, J. M. Raimundo, H. Dallaporta and A. M. Charrier, J. Mater. Chem. B., 2013, **1**, 443-446.
25. G.P. Li, G. Liu, Y.Z. Li, L. Hou, Y.Y. Wang and Z. H. Zhu, Inorg Chem., 2016, **55**, 3952-3959.
26. J.N. Hao, B. Yan, New J Chem., 2016, **40**, 4654-4661.
27. M. Chebeir, G. D. Chen and H. Z. Liu, Water Res. Technol., 2016, **2**, 906-914.
28. H. R. Fu, Z. X. Xu and J. Zhang, Chem. Mater., 2015, **27**, 205-210.
29. Q. Lu, C. L. Copper, G. E. Collins, Anal. Chim. Acta., 2006, **572**, 205-211.
30. G. Hamscher, B. Priess, H. Nau and E. Panariti, ACS Publications., 2005, **77**, 2421-2425.
31. T. M. Figueira-Duarte, K. Müllen, Chem Rev., 2011, **111**, 7260-7314.
32. X. Feng, J. Y. Hu, C. Redshaw and T. Yamato, Chem-Eur J., 2016, **22**, 11898-11916.
33. A. Ann. Laurent, Phys.,1837, **66**, 136.
34. C. Z. Wang, H. Ichiyanagi, K. Sakaguchi, X. Feng, M. R. J. Elsegood, C. Redshaw and T. Yamato, J. Org. Chem., 2017, **82**, 7176-7182.
35. M. Singh, M. Holzinger, O. Biloivan and S. Cosnier, Carbon., 2013, **61**, 349-356.
36. M. Bolognesi, S. Moschetto, M. Trapani, F. Prescimone, C. Ferroni, G. Manca and S. Toffanin, ACS Appl Mater Inter., 2019, **11**, 22637-22647.
37. Z. Zhao, J. W. Y. Lam and B. Z. Tang, J. Mater. Chem., 2012, **22**, 23726-23740.

38. M. A. Shameem, A. Orthaber, Chem-Eur. J., 2016, **22**, 10718-10735.
39. S. L. Tao, Y. C. Zhou, C. S. Lee, X. Zhang and S. T. Lee, ACS Publications., 2010, **22**, 2138-2141.
40. Y. N. Hong, J. W. Y. Lam, B. Z. Tang, Chem Soc Rev., 2011, **40**, 5361-5388.
41. E. Moulin, E. Busseron, N. Giuseppone, RSC, Cambridge., 2015, **2015**, 1-52.
42. M. El Idriss, S. J. Teat, P. F. X. Corvini, M. J. Paterson, S. J. Dalgarno and P. Shahgaldian, Chem. Commun., 2017, **53**, 1973-1976.
43. H. Nie, Y. Liang, C. Han, R. Zhang, X. Zhang and H. Yan, Dyes and Pigments., 2019, **168**, 42-48.
44. C. L. Deng, J. P. Bard, L. N. Zakharov and D. W. Johnson, Org. Lett., 2019, **21**, 6427-6431.
45. J. Hu, A. Paudel, T. Yamato, ChemInform., 2009, **40**, 109-113.
46. D. Chercka, S. J. Yoo, M. Baumgarten, J. J. Kim and K. Müllen, J Mater Chem C., 2014, **2**, 9083-9086.
47. R. J. Li, M. Li, X. P. Zhou, D. Li, M. O'Keeffe, Chem Commun., 2014, **50**, 4047-4049.
48. R. J. Li, M. Li, X. P. Zhou, S. W. Ng , M. O'Keeffe and D. Li, CrystEngComm., 2014, **16**, 6291-6295.
49. K. C. Stylianou, R. Heck, S. Y. Chong, J. Bacsa, J. T. A. Jones, Y. Z. Khimyak and M. J. Rosseinsky, J. Am. Chem. Soc., 2010, **132**, 4119-4130.
50. Q. L. Guan, Y. H. Xing, J. Liu, C. Han, C. Y. Hou, and F. Y. Bai, J. Phys. Chem. C., 2019, **123**, 23287-23296.
51. D. Shang, J. Ni, X. Gao, C. Li, X. Lin, Z. Wang and Y. Xing, New J Chem., 2016, **40**, 8100-8109.
52. T. Nozoe, H. Horino, T. Toda, Tetrahedron Lett., 1967, **52**, 5349-5353.
53. Y. Wang, Y. H. Xing, F. Y. Bai and L. X. Sun, Inorg Chem., 2018, **57**, 12850-12859.
54. W. Chen, Y. Zhuang, L. Wang, Y. Lv, J. Liu, T. L. Zhou and R. J. Xie, Interfaces., 2018, **10**, 18910-18917.
55. L. Wang, G. L. Fan, X. F. Xu, D. M. Chen, L. Wang, W. Shi and P. Cheng, J. Mater. Chem. A., 2017, **5**, 5541-5549.
56. J. Lu, X.H. Zhao, F.K. Zheng and G. C. Guo, J. Mater Chem C., 2019, **7**, 11099-11103.
57. J. Lu, H. F. Wu, W. F. Wang, J. G. Xu, F. K. Zheng and G. C. Guo, Chem. Commun., 2019, DOI:10.1039/C9CC06760D.
58. M. Brvar, T. Ploj, G. Kozelj, M. Mozina, M. Noc and M. Bunc, Crit Care., 2004, **8**, 56-59.
59. S. I. Weissman, J. Chem. Phys., 1942, **10**, 214-217.
60. N. Arnaud, E. Vaquer, J. Georges, The Analyst., 1998, **123**, 261-265.
61. B. L. Chen, Y. Yang, F. Zapata, G. N. Lin and G. D. Qian, Adv Mater., 2007, **19**, 1693-1696.
62. Z. M. Hao, X. Z. Song, M. Zhu, X. Meng, S. N. Zhao, S. Q. Su and H. G. Zhang, J. Mater. Chem., 2013, **1,** 11043.
63. J. N. Hao, B. Yan, J. Mater. Chem., 2015, **3**, 4788-4792.
64. J. M. Zhou, W. Shi, N. Xu and P. Cheng, Inorg Chem., 2013, **52**, 8082-8090.
65. W. Cheung, M. Patel, Y., Chen, Y. Ma, Q. Xie, J. V. Lockard and H. He, Chem Sci., 2016, **7**, 5192-5199.
66. D. Zych, A. Kurpanik, A. Slodek, A. Maroń, M. Pająk, G. Szafraniec-Gorol and W. Danikiewicz, Chem-Eur. J., 2017, **23**, 15746-15758.

View Article Online
DOI: 10.1039/C9NJ05175A

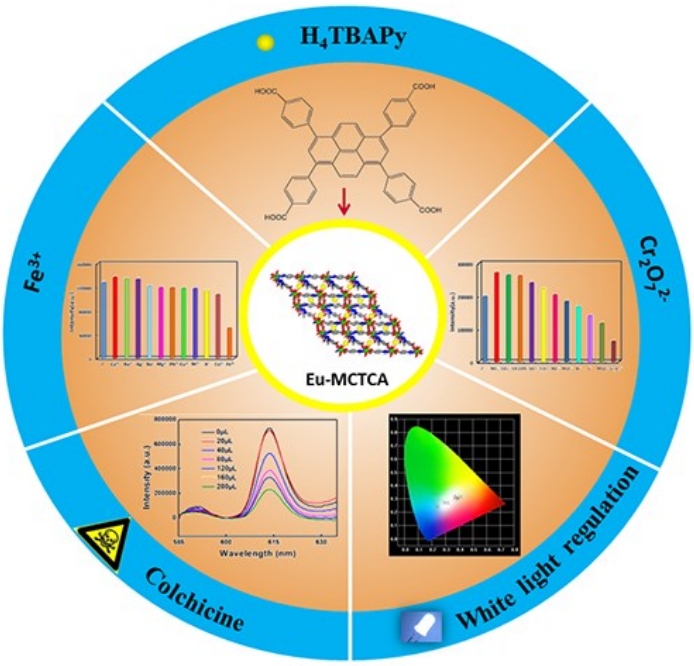

60x39mm (300 x 300 DPI)